Analytica Chimica Acta 1238 (2023) 340644

Contents lists available at ScienceDirect

Analytica Chimica Acta

journal homepage: www.elsevier.com/locate/aca

Sensitive electrochemical sensing platform based on Au nanoflower-integrated carbon fiber for detecting interleukin-6 in human serum

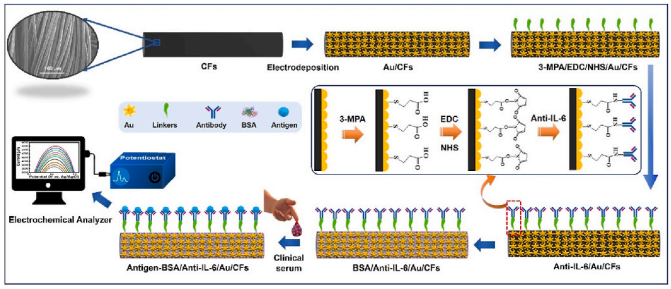
Sekar Madhu [a,1], Jang Hee Han [b,1], Chang Wook Jeong [b,c], Jungil Choi [a,*]

[a] Department of Mechanical Engineering, Ajou University, Suwon, 16499, Republic of Korea
[b] Department of Urology, Seoul National University Hospital, Seoul, 03080, Republic of Korea
[c] Department of Urology, Seoul National University College of Medicine, Seoul, 03080, Republic of Korea

HIGHLIGHTS

- A flexible carbon fiber-based electrochemical immunosensor is proposed for quantitative detection of prostate cancer biomarker, IL-6.
- The fabricated IL-6 immunosensor demonstrated higher sensitivity and a wide detection range with a lower detection limit of 0.05 fg/mL.
- The proposed low-cost fiber immunosensor is having the efficacy to detect the cancer biomarker in clinical serum at an early stage.

GRAPHICAL ABSTRACT



ARTICLE INFO

Keywords:
Prostate cancer
Carbon fiber
Gold nanostructure
Immunosensor
Cancer diagnosis
And flexible sensor

ABSTRACT

Prostate cancer (PCa) is the most prevalent cancer worldwide, with a high mortality rate. The early and accurate detection of PCa is critical in reducing mortality and saving lives. Timely diagnosis can improve the chances of successful treatment using advanced technologies. In recent years, nanomaterial-based electrochemical sensing strategies have been adopted in clinical diagnosis, as they allow sensitive early-biomarker detections to be converged with a cost-effective electronic readout system. Herein, we present a flexible electrochemical immunosensor platform for detecting interleukin-6 (IL-6) based on an Au-integrated flexible carbon fiber (Au/CF) electrode prepared via electrodeposition and chemically modified to capture IL-6 antibodies. Several techniques are used to analyze the prepared Au/CF composite electrodes to confirm their morphology, structure, and elemental composition. Under optimum conditions, the fabricated immunosensor exhibits a wide linear dynamic ranging from 1 fg/mL to 1 μg/mL and a low detection limit of 0.056 fg/mL, with a sensitivity of 62.17 μA/(fg mL^{-1}). The proposed fiber-based immunosensor is used to quantify the concentration of IL-6 in serum samples from clinical PCa patients (T3b and T4 stages), and the results are validated using the commercial Meso Scale Diagnostics (MSD) V-Plex method. The acceptable results yielded by the proposed immunosensor indicate that it can serve as a new platform to realize highly sensitive and cost-effective diagnostic strategies for the early diagnosis of PCa.

* Corresponding author.
E-mail address: cji@ajou.ac.kr (J. Choi).
[1] These authors contributed equally to this work.

https://doi.org/10.1016/j.aca.2022.340644
Received 1 August 2022; Received in revised form 11 October 2022; Accepted 17 November 2022
Available online 18 November 2022
0003-2670/© 2022 The Authors. Published by Elsevier B.V. This is an open access article under the CC BY license (http://creativecommons.org/licenses/by/4.0/).

1. Introduction

A recent survey by the American Cancer Society reported that prostate cancer (PCa) is the most frequently diagnosed cancer and the second most prominent cause of mortality among men after lung cancer [1,2]. As PCa is a moderately slow-growing cancer, establishing an effective early diagnosis protocol can help initiate early treatment, which would improve the chances of successful therapeutics. Timely treatment can reduce the rate of metastasis to other sites and increase the survival rate [3,4]. The growth of PCa to a metastatic state along with hormone independence is a multistep process involving hormones, growth factors, and cytokines [5–7]. Prostate-specific antigen (PSA) is a Food and Drug Administration ratified serum biomarker that is currently employed for the diagnosis of PCa [8]. Although the use of PSAs as a PCa biomarker is controversial in some patients, it fails to distinguish prostate carcinoma from benign prostate hyperplasia, prostatitis, and cystitis [9,10], all of which can increase PSA levels. Consequently, identifying alternate PCa biomarkers to improve detection selectivity and clinical manifestation is extremely challenging to the research community [8]. Interleukin-6 (IL-6), a cytokine with diverse biological roles, is vital to the growth of PCa [5,10]. IL-6 is a glycoprotein secreted by lymphocytes, macrophages, monocytes, fibroblasts, endothelial cells, and some tumor cells [11,12]. Overexpression of serum IL-6 is linked to the process of cancer, which promote the proliferation and metastatic potential of cancer cells in particularly it activates androgen receptor (AR) in PCa [13,14]. IL-6 activates in PCa pathways of Janus kinases/signal transducers and activators of transcription (STAT), mitogen-activated protein kinases, and phosphatidylinositol 3-kinase. IL-6 stimulates the growth of prostate cancer cells via autocrine and/or paracrine mechanisms and might contribute to tumor escape from immune surveillance, resulting in disease progression through the increased production of IL-6. Moreover, increasing evidence shows a correlation between IL-6 with the progression of PCa and targets IL-6 for therapeutics in clinics. V. Michalak et al., reported about the baseline serum levels of cytokines in healthy and PCa patients and the prognostic significance with the cut off value $>$ 2.1 pg/mL of serum IL-6 affects their survival rate [5,15]. Hence, reliable diagnostic tools for detecting IL-6 can be used as an alternative tool for the point-of-care (POC) sensing of PCa [8,16].

State-of-the-art techniques such as immunoblotting, radioimmunoassay, polymerase chain reaction, immunohistochemistry, high-performance liquid chromatography (HPLC), western blotting, and enzyme-linked immunosorbent assay (ELISA) [17–21] are widely used for the clinical measurement of IL-6. Although HPLC and ELISA can be routinely performed by trained technicians still these methods have some limitations. In HPLC, the usage of large quantity expensive chemicals increases the cost of analysis. Also, it has low sensitivity for certain compounds, and some cannot be detected as they are irreversibly adsorbed. In the case of ELISA, the demand for the large sample volume (100–200 μL) in 96-well plate limits the accurate target quantification and reliable outcomes. This induce the possibility of false-positive or negative results is high in ELISA due to insufficient blocking of immobilized antigen [1]. In addition, the cost and turnaround time restrict its practical feasibility in early diagnosis and community screening of IL-6. Conversely, the electrochemical immunosensors are the predominant alternative to these conventional techniques and exhibit high potential for real sample analysis owing to their high selectivity, sensitivity, accuracy, low detection limits, and quick response [3].

In a typical electrochemical immunosensing setup, the output electrical signals, such as current, potential, or resistance, can be directly processed using a portable electronic readout system, which facilitates the miniaturization of the overall components into wearable or self-monitoring device modules [22,23]. Further, the conventional electrodes used in the electrochemical sensor applications, including Pt, Au, glassy carbon electrodes (GCEs) and printed electrodes, are cost prohibitive and subject to variability [24]. Also, the self-oxidation and internal resistance are easily influencing the electrochemical activity of the sensor. The recent trend in fabricating cost-effective electrochemical sensors is shifting toward paper and ceramic electrodes, as well as flexible sensor fabrication using printing approaches. We have previously reported a carbon yarn-based electrode as an alternative electrode for the electrochemical biosensing of clinically important biomarkers [25,26]. The direct growth of active materials on flexible substrates, such as carbon fibers (CFs), is an alternative strategy which substrate yields three-dimensional network structures, providing open channels for efficient electron/ion transport and a large surface area for reactions, both of which are beneficial to electrochemical devices. Furthermore, it overcomes the disadvantages of combining the active electrode materials with conductive additives and binders that evades the problems including the “dead-surface” associated with conventional slurry-derived substrates and enhances the electron transport and simplify electrode processing [27,28].

CFs, an outstanding type of carbon material, have been widely applied in electrochemistry owing to their excellent conductivity, intrinsic carrier mobility, high mechanical stability, and low cost. They have garnered substantial attention as a flexible electrode material for biological and chemical applications. However, electroactive sites on CFs are moderate, thus resulting in low electrocatalytic performance toward analytes [25,29]. Among potential nanofunctional materials, Au nanoparticles are illustrious components that are the most typically used in electrochemical sensors owing to their large surface-area-to-volume ratio, in addition to their rich functionalization strategy, strong protein adsorption, high surface free energy, excellent biocompatibility, and high conductivity [30,31]. Various approaches have been employed to deposit Au nanomaterials onto sensor surfaces. Among them, the electrodeposition of Au is a promising method as it allows uniform depositions via cost-effective, simple, and scalable operational steps [8,29].

Song et al. prepared uniform Au nanoflower-based composites on CF microelectrodes for the sensitive detection of serotonin. The composite material exhibits a wide dynamic range, a low detection limit, and antifouling performance toward serotonin because of the incorporation of a large surface area, electrochemically conductive Au nanostructures, and overoxidized polypyrrole [32]. Zhang et al. utilized the Au nanoflower/peptide nucleic acid-modified CF microelectrode as electrochemical platform for detecting circular RNAs. The modified platform exhibited a linear range of 10 fM to 1 μM with a minimum detection limit of 3.29 fM [33]. Zhangquan et al. developed a novel electrode substrate that uniformly electrodeposited Pt–Au nanocatalysts on the surface of reduced-graphene-oxide-wrapped CFs. The prepared composite electrode showed high catalytic activity and stability toward formic acid electrooxidation [34]. These studies indicate that Au/CFs are suitable for detecting various biomarkers and electrolytes. Currently, electrochemical sensors based on Au nanoflower-modified CFs for determining IL-6 serum samples from patients with PCa have not been reported.

Herein, we propose a conductive fiber-based electrochemical immunosensor for the highly sensitive detection of IL-6 in serum samples for the first time. Au nanoflowers were uniformly electrodeposited onto a flexible CFs to immobilize IL-6-specific antibodies through cross-linking chemistry. Cyclic voltammetry (CV) and differential pulse voltammetry (DPV) are employed for the electrochemical analysis of the immunosensor. The IL-6 detection mechanism relies on immunocomplex formation on the sensing surface, which hinders ion exchange with the redox probe. Owing to the anchoring of Au nanostructures onto CFs without the aid of any binders/additives, the sensing platform offers highly active redox sites, which subsequently result in higher sensitivity, excellent stability, and higher selectivity. Furthermore, the fabricated immunosensor was evaluated to quantify IL-6 levels in human PCa patient serum samples, and the results were validated using the commercial MSD V-Plex method. Hence, the applicability of the sensor for integration into wearable sensor modules is confirmed.

2. Materials and methods

2.1. Materials

The commercial carbon cloth (CC) (20 cm × 20 cm × 0.36 cm) was directly purchased from Nara Celltech Corp (Seoul, South Korea). Gold (III) chloride trihydrate ($HAuCl_4{\cdot}3H_2O$), 3-Mercaptopropionic acid (3-MPA), *N*-hydroxysuccinimide (NHS), 1-(3-(dimethylamino)-propyl)-3-ethyl carbodiimide hydrochloride (EDC), Sulfuric acid, Bovine serum albumin (BSA), Potassium ferricyanide, Potassium chloride (KCl), Human carcinoembryonic antigen (CEA), Interleukin-8 (IL-8), Interleukin-10 (IL-10), Procalcitonin (PCT), Human serum albumin (HSA), Prostate-specific antigen (PSA), IgG serum, and Cytochrome *c* (Cytc) were purchased from Sigma. Alpha-Fetoprotein (AFP) was purchased from Leehyo Bioscience, South Korea. The human IL-6 antigen, monoclonal anti-IL-6 antibody (Ab), and phosphate-buffered saline (PBS) were procured from Thermo Fisher Scientific. All other chemicals used were of analytical reagent grade and used without further purification. Aqueous solutions were prepared using deionized (DI) water (ρ = 18.2 MΩ cm) from a Millipore Milli-Q system.

2.2. Pretreatment of CFs

Prior to electrodeposition, the CFs (5 cm long) were subjected to 30 min of ultrasonication in ethanol and DI water. Subsequently, the cleaned CFs were treated in a mixture comprising concentrated HNO_3 and H_2SO_4 solutions (at a ratio of 1:3) at 70 °C for 3 h to improve their hydrophilicity and to develop adequate adhesion between the surfaces of carbon and active material. Subsequently, they were rinsed with DI water to remove residues and then dried in an oven at 60 °C for 12 h.

2.3. Preparation of Au-electrodeposited CFs

Au nanoflowers were deposited on chemically treated CFs via a single-potential-step electrodeposition process. An electrolyte solution containing 5 mM $HAuCl_4{\cdot}3H_2O$ in 0.5 M H_2SO_4 was used for the deposition process, and a constant potential of −0.2 V was applied for 30 s. During this process, the chemically modified CFs were used as the operating electrode, whereas a Pt wire and Ag/AgCl were used as the counter and reference electrodes, respectively. The effect of morphological features with respect to the deposition time and length of the Au/CFs along with their corresponding electrochemical responses are provided in Figs. S1–S3. The resultant Au-deposited CFs were rinsed with DI water and ethanol several times to eliminate any physically adsorbed $AuCl_4$ ions and then exsiccated at 60 °C. Details regarding the materials and reagents used in this study are provided in the supporting information.

2.4. Step-wise fabrication of anti-IL-6/Au/CF immunosensor

The derivatization procedure for preparing the immunosensor is shown schematically in Fig. 1. Initially, the Au/CF electrodes were incubated in 10 mM 3-Mercaptopropionic acid (MPA) for 1 h, which formed a self-assembled monolayer through Au–SH bond formation [35]. Subsequently, the electrodes were incubated in PBS (10 mM, pH 7.4) containing 400 mM EDC (used as a coupling agent) and 400 mM NHS (used as an activator) hybrid solution for 40 min to activate the surfaces of the MPA-modified electrode. Next, the NHS ester-functionalized Au/CF composite electrode was immersed in an IL-6 antibody solution (80 μL, 10 mM PBS, pH 7.4) for 150 min for the covalent coupling of the antibodies on the electrode surfaces through stable amide bond formation. Unbound antibodies on the Anti-IL-6/Au/CF electrodes were removed via washing in PBS prior to incubation with 60 μL of 2 wt% BSA for 30 min to barricade the nonspecific binding sites of Anti-IL-6. Finally, the BSA/Anti-IL-6/Au/CF immunoelectrode was washed with PBS to remove the unbound BSA and then incubated at 4 °C. The detailed electrochemical sensing mechanism of the proposed immunosensor is provided in the supporting information (Fig. S5).

2.5. Material characterizations

The morphology and elemental composition distribution of the prepared Au/CF nanocomposite were examined using field-emission scanning electron microscopy equipped with energy dispersive spectroscopy (FESEM-EDS; JEOL JSM-7610F). The structural properties were analyzed via X-ray diffraction (XRD, Rigaku Ultima IV) with Cu–Kα radiation (λ = 1.5406 Å) at 40 kV. The surface chemistry of the prepared nanocomposite was analyzed using X-ray photoelectron spectrometry (XPS, Multilab 2000, UK) combined with Al–Kα radiation.

2.6. Electrochemical measurements

All electrochemical measurements were performed using a PalmSens4 portable potentiostat in the presence of 5 mM $[Fe(CN)_6]^{4-/3-}$ as a redox probe in 10 mM PBS. CV measurements were conducted in the optimized potential range of −0.2–0.8 V (*vs.* Ag/AgCl) at a scan rate of 50 mV/s. DPV was performed for the sensitive electrochemical detection of IL-6 based on an optimized potential window of −0.2 to 0.6 V *vs.* Ag/AgCl, a step potential of 5 mV, pulse amplitude of 50 mV), and a pulse

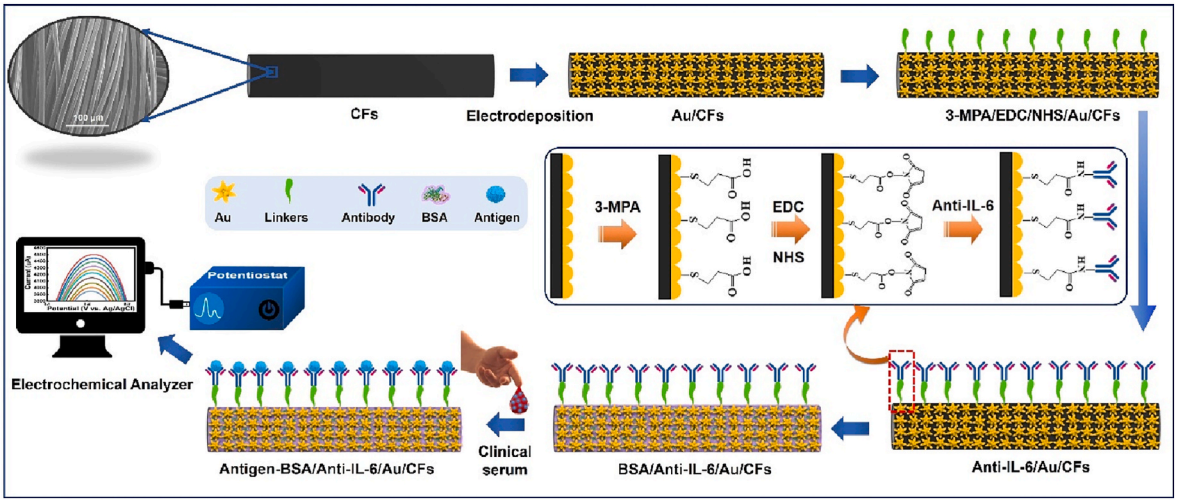


Fig. 1. Outline of IL-6 immunosensor design. Schematic illustration of fabrication sequences of IL-6 immunosensor and its electrochemical responses toward IL-6.

period of 0.01 s. All measurements with an analyte were recorded with a 5 min incubation time.

2.7. Sample acquisition and processing

Blood samples (2 mL) were clinically obtained from 28 patients aged between 45 and 70 years with stage-T3b and -T4 PCa (diagnosis was confirmed histopathologically) from Seoul National University Hospital, South Korea. To avoid the effects or alter the levels of IL-6, blood sampling was completed prior to the administration of any treatment. Patient consent was obtained prior to sampling, and all recommendations about the handling of actual samples obtained from human subjects by the Institutional Review Board (IRB) of Seoul National University Hospital (IRB no. 2103-213-1209) were considered. Samples were stored in sterilized plastic containers and then centrifuged at 3000 rpm for 10 min following not more than 30 min after sampling. The supernatant obtained after centrifugation (serum) was collected, transferred to sterilized plastic containers, and stored at −80 °C until electrochemical measurements were performed.

3. Results and discussion

3.1. Physical characterizations

Fig. 2a–h shows the distinctive surface morphology and element distribution of the Au-deposited CFs analyzed using FE-SEM. The pristine CFs comprised small fibers with an average diameter of 10 μm (Fig. 2a). The different magnifications of the FE-SEM images revealed the formation of well-aligned flower-like Au nanostructures with a mean diameter of ~100 nm on the frames of the CFs (Fig. 2b and c). The corresponding EDS spectrum of the Au/CF modified electrode shown in Fig. 2d confirmed that the synthesized Au/CF nanoflowers contained Au (59.5%), C (38.4%), and O (2.16%). The presence of a minute amount of oxygen in the Au/CFs suggests the formation of oxygen-containing hydroxyl and carboxyl groups on the Au surface. The EDS elemental mapping shown in Fig. 2e–h clearly reveals the consistent spatial distributions of Au, C, and O without any self-aggregation, indicating that the Au nanoflowers were uniformly distributed on the surfaces of the CFs. In addition, the absence of any other peaks/elements exemplified the absence of impurities in the prepared composite material. The detailed EDS analysis of bare, acid-treated, and Au-integrated CFs are shown in Fig. S4.

The phase purity and crystalline structure of the pristine and Au/CF nanocomposite electrodes were examined via XRD (Fig. 2i). Two diffraction peaks were observed at $2\theta = 25.6$ and 43.2°, which correspond to the (002) and (101) crystalline planes of the hexagonal structure of the CF substrate, respectively, [36]. For the Au/CFs, four additional diffraction peaks appeared at 38.1, 44.3, 64.5, and 77.7°, which correspond to the (111), (200), (220), and (311) diffraction of the face-centered cubic phases of Au (JCPDS 01–1172), respectively, thus confirming that Au was successfully integrated onto the CFs [31]. No additional peaks other than those of Au and the carbon were observed, which indicates the high purity of the prepared Au/CF composites. The crystalline size of the Au-electrodeposited CFs was measured using Scherrer's formula and was calculated to be ~12 nm.

XPS analysis was performed to identify the apparent elemental status and characteristics of the chemical bonding of the prepared flexible Au/CFs substrate. As shown in Fig. 2j, the survey XPS spectrum reveals the presence of Au, C, and O elements. Based on the deconvoluted C1s spectrum of Au/CFs shown in Fig. 2k, the unoxidized graphitic carbon can be assigned to 284.7 eV (C–C), whereas the presence of carbon in the hydroxyl and epoxy groups can be assigned to 286.3 eV (C–O) and that in the carboxyl group to 288.7 eV (C═O) [37]. In Fig. 2l, the $Au^{(0)}$ oxidation state emerges owing to the spin–orbit split between peak positions of the energy band observed in the core level XPS spectrum of Au at 83.8 eV (Au 4 $f_{7/2}$) and 87.5 eV (Au 4 $f_{5/2}$). The absence of a peak corresponding to $Au^{(III)}$ at a binding energy of ~92 eV confirmed the complete reduction of $Au^{(0)}$ on the sidewalls of the Au/CFs [38]. As shown in Fig. 2m, from the three characteristic peaks of O 1s spectrum, the core intense peak at 532.2 eV is ascribed to C–O, and the other two small shoulder peaks at the binding energies of 530.3 and 533.9 eV are identified to the surface traps C═O and O–C═O bands respectively [39]. The FE-SEM images, EDS analysis, and XRD and XPS spectra results collectively confirmed that the flower-like Au nanostructures accumulated uniformly on the CFs, and that the electrodeposited materials were composed of Au, with no indications of metal impurities other than carbon.

3.2. Electrochemical characterizations of anti-IL-6/Au/CF immunosensor

As an effectual method for evaluating the electrochemical performance of the fabricated electrodes, CV measurements were conducted in a 10 mM PBS (pH 7.4) containing 5 mM $K_3[Fe(CN)_6]$ as an electrochemical redox probe. As shown in Fig. 3a, reasonably weak responses of the reversible redox peaks were observed for the pristine CF electrodes. This is characteristic of CFs and is attributable to their low electron conductivity (black curve: CFs). After the electrodeposition of Au onto the CFs, the redox peaks resulting from the redox reactions of $[Fe(CN)_6]^{3-/4-}$ were higher than those of the pristine CFs. The higher redox peak currents exhibited on the Au/CFs as compared with those of the bare CFs are attributed to the following reasons: Au is a conductive metal nanomaterial and can improve the electrode active surface area considerably, and the incorporation of Au nanostructures onto CFs provides large electrochemical active sites, thus facilitating the transfer of electrons between the electrode and electrochemical probe (red curve: Au/CFs). Conspicuous changes occurred after the subsequent immobilization of IL-6 antibody binding, where the electrochemical redox currents decreased significantly. This is because of the large size of the protein and its effective immobilization of Anti-IL-6 with the Au-modified CFs platform (blue curve: Anti-IL-6/Au/CFs). The final step of free-site blockage via the neutral protein of BSA shows a slight decrement in the electrochemical redox peak currents, suggesting the formation of a densely packed biolayer on the non-binding sites of Anti-IL-6 on the Au/CFs, which can hinder electron transfer. The obstruction of nonspecific binding sites on the modified electrode surface is the most imperative step during immunosensor fabrication, as it prevents nonspecific interactions on the immunoelectrode (green curve: BSA/Anti-IL-6/Au/CFs).

3.3. pH effect of supporting electrolyte

The pH of the supporting electrolyte affects the electrochemical performance of immunosensors. An unsuitable solution pH may result in the denaturation of the antibody. To confirm the optimal pH, the immunosensors were tested via the CV (scan rate 50 mV/s) method in the presence of constant IL-6 concentrations while varying the solution pH from 4.0 to 9.0. The immunosensor indicated a maximum electrochemical current response at pH 7.4, and an increase in pH resulted in a decrease in the redox peak current (Fig. 3b and S6). Based on the CV results indicating that highly acidic or alkaline solutions may adversely affect the bioactivity of immobilized proteins, pH 7.4 was selected for the IL-6 detection process to obtain the maximum sensitivity.

3.4. Effect of scan rate on peak currents of IL-6

The CV measurements were performed to determine the factor that controls the electrochemical process on the prepared BSA/Anti-IL-6/Au/CF immunosensor by varying the scan rate from 10 to 100 mV/s in PBS (10 mM, pH 7.4). Fig. 3c shows a slight peak shift in the oxidation peak current response toward a higher potential and a reduction in the peak current near the lower potential as the scan rates increased from 10 to 100 mV/s. Both the anodic peak current (I_{pa}) and cathodic peak current

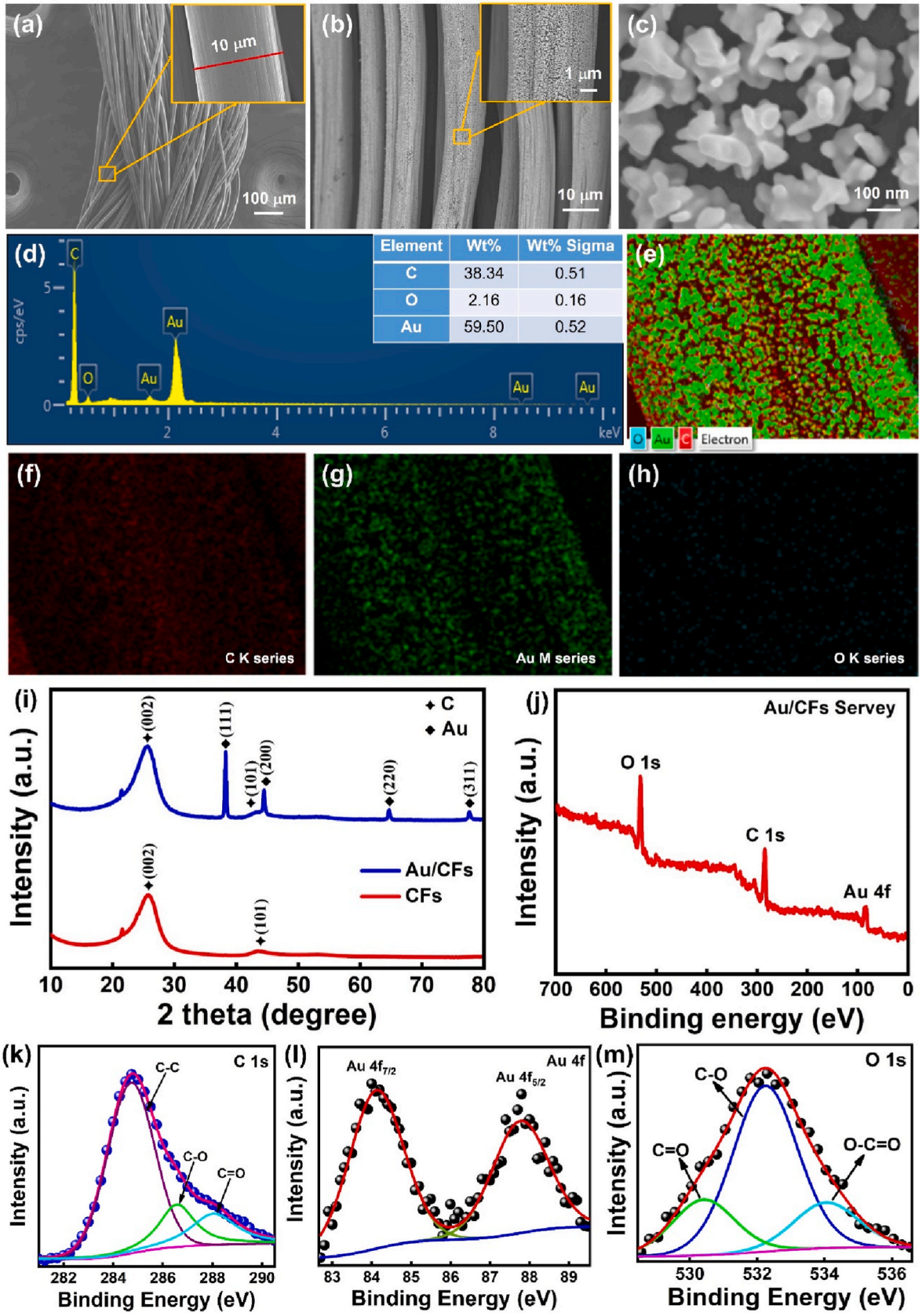


Fig. 2. Analytical characterizations of pristine and Au/CF nanocomposites. FE-SEM images of (a) pristine CFs and (b, c) Au-integrated CFs with different magnifications. (d) EDX spectrum (e–h) elemental mappings. (i) XRD spectra, and (j–m) XPS analysis of Au/CFs.

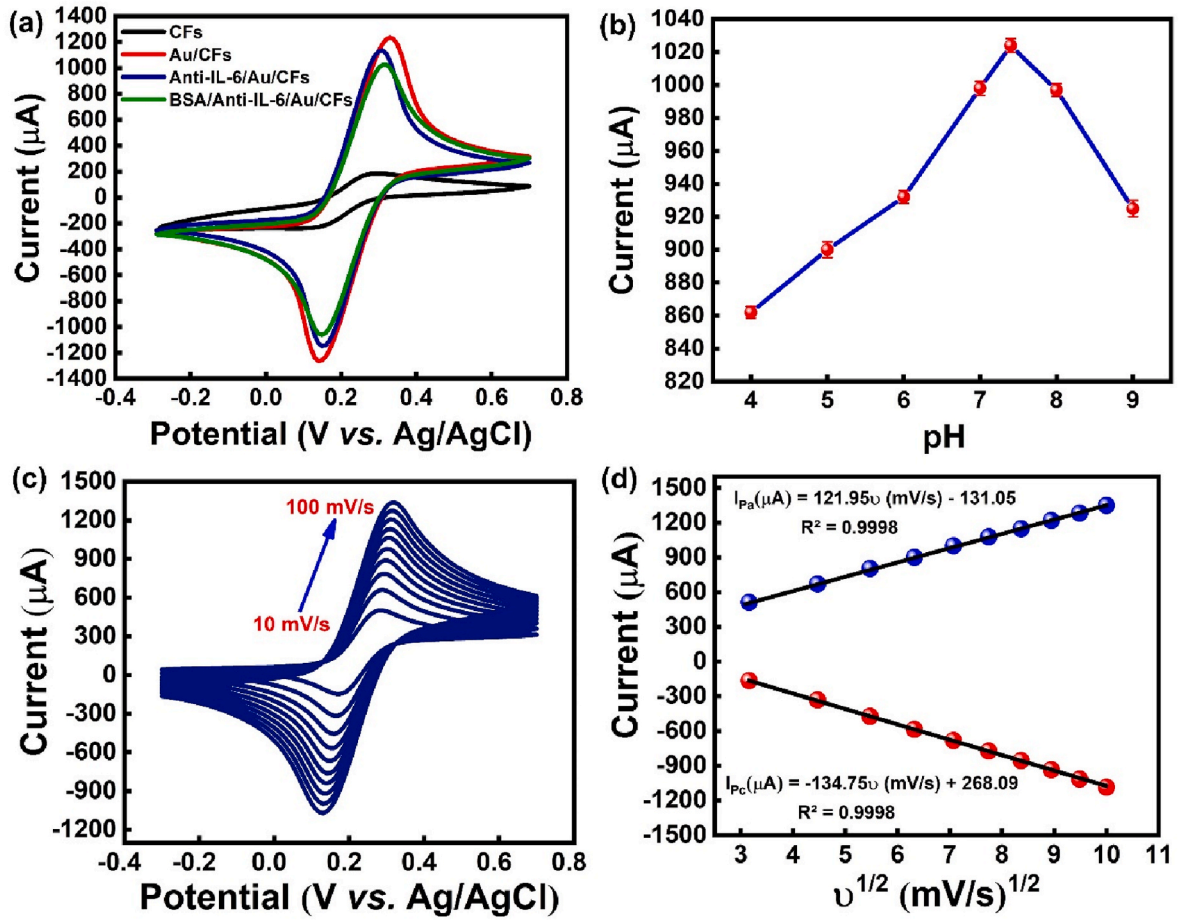


Fig. 3. Construction of Au/CF based IL-6 immunosensor platform and their basic electrochemical characterizations. (a) CV analysis of step-wise modification of immunoelectrode in 10 mM PBS solution containing 5 mM $[Fe(CN)6]^{3-/4-}$. (b) Plot of oxidation peak currents *vs.* pH. (c) CV measurements of BSA/Anti-IL-6/Au/CF immunoelectrode by varying scan rates (10–100 mV/s). (d) Calibration plot of electrochemical current responses *vs.* square root of scan rate.

(I_{pc}) increased linearly and proportionally to the square root of the scan rate, indicating that the prepared immunoelectrode reaction was a diffusion-controlled process, as shown in Fig. 3d. The corresponding regression equations are shown in Eqs. (1) and (2).

$$I_{pa}(\mu A) = 121.95\ v^{\frac{1}{2}}\ (mV/s) - 131.05;\ R^2 = 0.999 \quad \text{(Eq.1)}$$

$$I_{pc}(\mu A) = -134.75 v^{\frac{1}{2}}\ (mV/s) - 268.09;\ R^2 = 0.999 \quad \text{(Eq.2)}$$

The separation of peaks shows that the electrochemical reaction is not ideally reversible, and the stable redox electrochemical peak current and position during repeated scans at a specific scan rate indicate that the fabricated immunoelectrode exhibited a quasi-reversible process [22].

3.5. Calculation of assessable surface area of CFs based modified electrodes

Measurement of the electroactive surface area (A_e) of the CFs modified electrodes is important to explicate the electrochemical efficacy of the electrode surface towards the bioactive molecules and it was calculated using the Randle's Sevcik equation as displayed in Eq. S1 and Fig. S7 [30]. The value of A_e for bare CFs and Au/CFs was found to be 0.065 and 1.85 cm^2, respectively. Au nanostructures efficiently enhance the effective surface area of the CFs, which improves the conductivity and enables immobilized biomolecules on the sensing electrode by bio-conjugation. After modified with IL-6 antibodies and BSA on the Au/CFs, the redox current responses decreased which might be due to the IL-6 antibody and BSA occupied the Au/CFs limits the charge transfer. Therefore, the A_e value reduced to 1.68 and 1.52 cm^2 compared to Au/CFs (1.85 cm^2). The values are tabulated as Table S1.

3.6. Detection of IL-6 using fiber-based immunosensor via CV and DPV

Under the optimized conditions, the electrochemical performance of the BSA/Anti-IL-6/Au/CF immunosensor was investigated based on various concentrations of IL-6 via CV and DPV. Fig. 4a shows the CV curves of the immunosensor prepared with various concentrations of IL-6 in PBS (10 mM, pH 7.4). As expected, the electrochemical current response declined with logarithmic IL-6 concentrations from 1 fg/mL to 1 μg/mL because the antigen-antibody complex served as an inert block layer that hindered electron transfer toward the modified electrode surface. The corresponding calibration plot for the oxidation peak currents vs. the logarithmic IL-6 concentrations is shown in Fig. 4b. The regression equation for the linear plot is expressed as shown in Eq. (3).

$$I\ (\mu A) = -15.956x + 758.12\ Log[IL-6\ Conc.\ (g/mL)];\ R^2 = 0.999 \quad \text{(Eq.3)}$$

The prepared fiber-based immunosensor exhibited a wide linear response to IL-6 concentration with a correlation coefficient of 0.999 and a sensitivity of 15.9 μA/(fg mL^{-1}). The low detection limit (LOD) of the BSA/Anti-IL-6/Au/CF immunosensor was estimated to be 1 fg/mL using the 3σb/m criterion, where σb is the estimated standard deviation of the y-intercepts of the regression curve, and m is the slope of the calibration curve.

Subsequently, we investigated the analytical performance of the

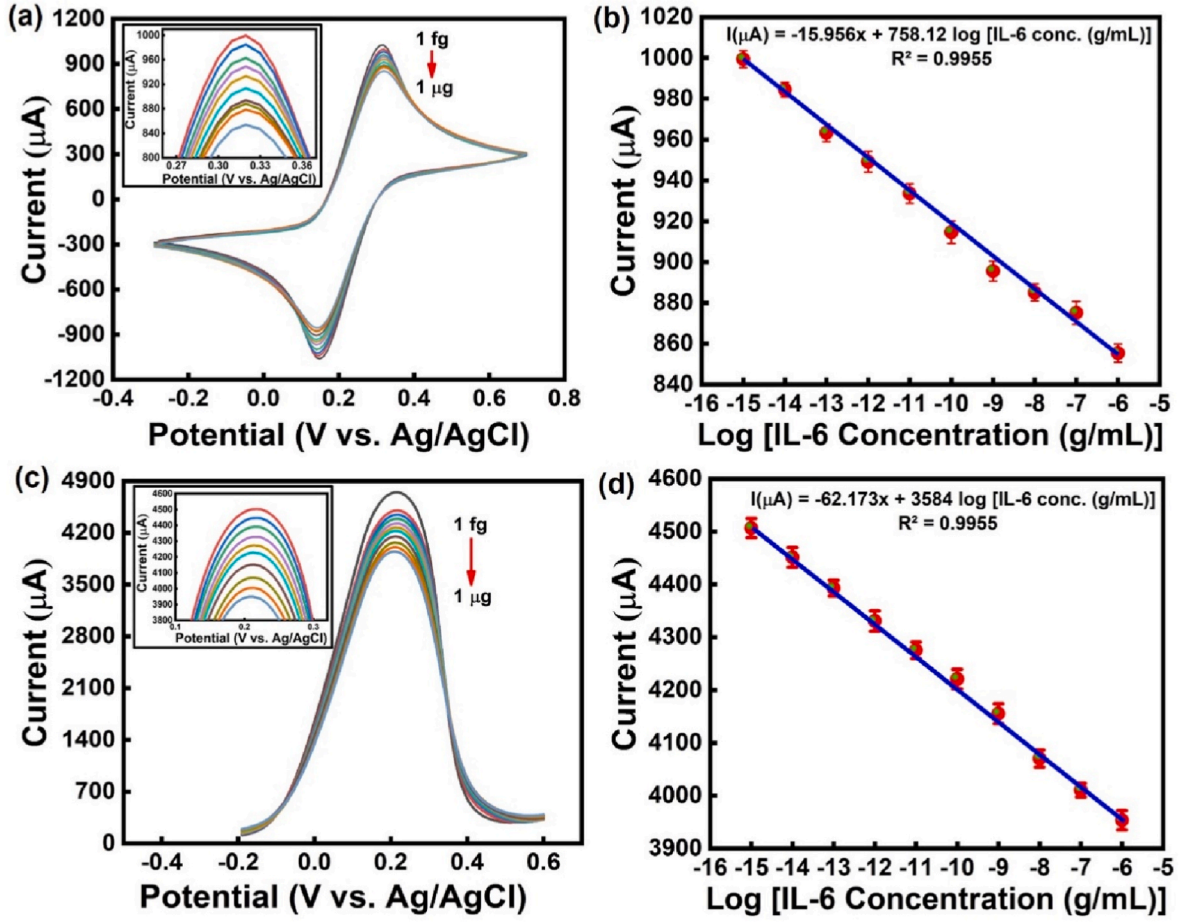


Fig. 4. Electrochemical performance of Au/CFs modified immunosensor toward IL-6 detection. Measurement of various concentrations of IL-6 (1 fg/mL to 1 μg/mL) using BSA/Anti-IL-6/Au/CF immunosensor via (a) CV and (c) DPV, (b,d) calibration plot of electrochemical current response vs. logarithmic concentrations of IL-6. (Inset: magnified view of CV and DPV curves showing variations in signal output due to IL-6 binding).

BSA/Anti-IL-6/Au/CF immunosensor using the sensitive analytical DPV method, as it is suitable for signal amplification, particularly when the analyte concentration is extremely low [40]. Under optimal conditions, the electrochemical oxidation peak current of the DPV curves progressively decreased when the IL-6 analyte concentration increased, which suggests the formation of an antigen-antibody complex that prevented current flow, as shown in Fig. 4c. The DPV responses of the BSA/Anti-IL-6/Au/CF immunosensor exhibited a linear relationship with logarithmic IL-6 concentrations ranging from 1 fg/mL to 1 μg/mL, as illustrated in Fig. 4d. The linear regression equation is shown in Eq. (4), and the LOD was calculated to be 0.056 fg/mL, with a sensitivity of 62.17 μA/(fg mL^{-1}). The detailed calculation of LOD is provided in Table S2.

$$I\ (\mu A) = -62.173x + 3548\ Log[IL-6\ Conc.\ (g/mL)];\ R^2 = 0.996 \quad \text{(Eq.4)}$$

3.7. Interference, reproducibility, repeatability, and stability analysis

Another important aspect is selectivity, as nonspecific binding at the sensor surface yields a false signal and results in misleading results. Since the human serum is a complex mixture of proteins that exhibit structural resemblances, the constructed immunosensors should be able to identify the target and quantitatively analyze its concentration in the sample.

As a result, the proposed immunosensor's selectivity was tested using common interfering proteins such digestive enzymes and tumor markers. As shown in Fig. 5a, the electrochemical current values corresponded to the simultaneous addition of 100 pg/mL of each interference (at a level higher than normal physiological concentrations), such as CEA, IgG, IL-8, Cytc, IL-10, PCT, HSA, AFP, PSA, and IL-6 (100 pg/mL). The results show no significant effect on the BSA/Anti-IL-6/Au/CF immunosensor response due to other non-target compounds, thus indicating the excellent selectivity of the proposed immunosensor.

The reproducibility of the sensor performance was evaluated for eight independently prepared BSA/Anti-IL-6/Au/CF immunoelectrodes using the CV method in a PBS (10 mM, pH 7.4) solution containing 100 pg/mL of IL-6, as shown in Fig. 5b. The magnitude of the electrochemical current was measured meticulously for each electrode, and the relative standard deviation (RSD) was evaluated subsequently. Owing to the simplicity of the material preparation and immobilization, the fabricated immunosensor showed an RSD of 1.8%, which suggests the reproducibility of the developed strategy.

The repeatability of the BSA/Anti-IL-6/Au/CF immunosensor was investigated via 10 continuous trials using a single immunoelectrode in the sensing of 100 pg/mL IL-6 in PBS (10 mM, pH 7.4). No noticeable deviation was indicated in the oxidation peak current responses obtained for the 10 Au/CF immunoelectrodes, and the significant RSD was 1.1%, as shown in Fig. 5c. This consistency in the current behavior reveals the repeatability of the designed electrochemical sensor, rendering it a reliable sensing platform for IL-6 detection.

Successively, the long-term storage stability of the proposed immunosensor was evaluated by intermittently measuring the electrochemical current in PBS (10 mM, pH 7.4). For this, the BSA/Anti-IL-6/Au/CF immunosensor was stored in a refrigerator (4 °C) at dry state for 6 weeks, and its self-life was investigated. An approximately 10% decrease in the electrochemical current response was found, and the

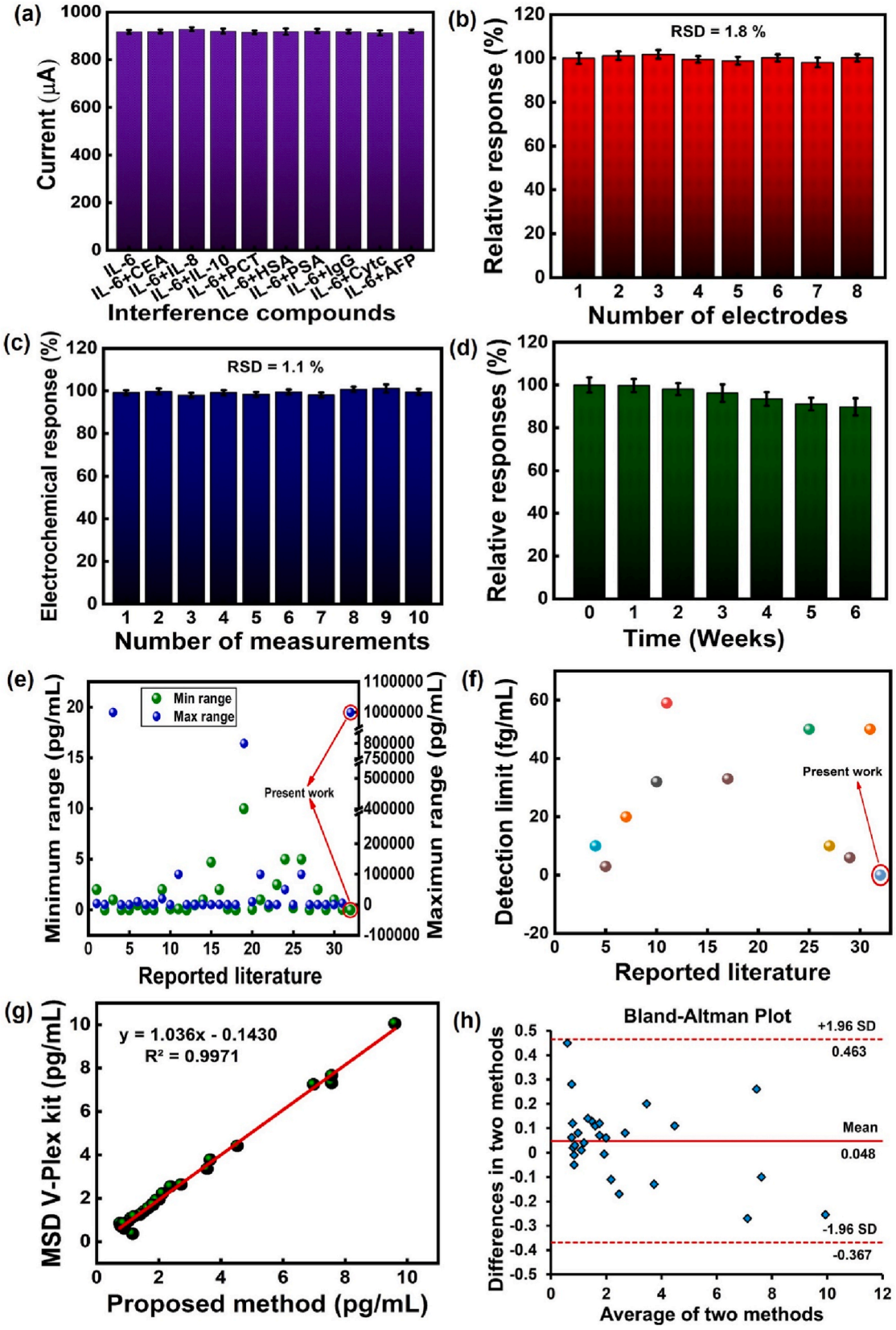


Fig. 5. Electrochemical performance of immunosensor and clinical validation for IL-6 determination based on serum from patients with prostate cancer. (a) Selectivity, (b) reproducibility, (c) repeatability, and (d) stability of BSA/Anti-IL-6/Au/CF immunosensor toward IL-6. (e and f) Comparison plots of dynamic ranges and detection limit between the proposed immunosensor and previous devices toward IL-6 detection. (g) Correlation between results obtained using proposed strategy and MSD V-Plex kit (n = 28) in determining IL-6. (h) Bland–Altman analysis showing good agreement between the proposed immunosensor and a commercial reference method for IL-6, with a low mean bias and all points within ±1.96 S.D. $p > 0.05$ indicates that the two methods are not statistically different.

corresponding image is shown in Fig. 5d. Similarly, the stability of the immunosensor in the successive 100 cycles potential scans was examined in 10 mM PBS, which resulted in a 1.1% decrease in its initial electrochemical current response even after 100 continuous trials (as shown in Fig. S8). These results suggest the consistent stability of the immunosensor owing to the adhesion between the Au sensing material and CF substrate, which is one of the primary considerations when assessing the overall stability and repeatability of the sensing system. In addition, the direct growth of Au-active materials on the CF flexible substrates without conductive additives and binders improved the long-term stability of immunosensors.

Compared with other previously reported IL-6 sensors, the proposed flexible immunosensor presents a satisfactory detection limit and linear range, and the results yielded by it are summarized in Fig. 5e and f and Supplemental Table S3. The high sensitivity and wide linear range of the proposed immunosensor are attributable to the uniform deposition of Au nanostructures onto the CFs, thereby affording excellent conductivity, large surface-active sites for greater antibody immobilization, and good biocompatibility, which can consequently amplify the electrochemical signal.

3.8. Real sample analysis

The assessment of immunosensor proficiencies based on real samples must be verified to prove their practical feasibility for POC and clinical applications. Blood samples were obtained from 28 patients with stage-T3b and -T4 PCa. These stages in PCa pose significant issues in radiotherapy methods owing to the wider target volume outside the prostate [41]. The samples obtained were labeled P1 to P28. After centrifugation, the obtained supernatant (serum) was collected and placed in sterilized plastic containers for further electrochemical examination. Primary tests were performed on undiluted serum samples, but the recovery rates were low. Therefore, the serum samples were diluted with 10 mM PBS (pH 7.4) at a ratio of 1:1. For a typical analysis, the fiber-based immunosensor was incubated with 20 μL of the serum samples for 15 min at 25 °C in a humid environment to avoid solvent evaporation, rinsed thrice before being placed into the electrochemical cell, and tested in a 5 mM $[Fe(CN)_6]^{3-/4-}$ PBS (10 mM, pH 7.4) solution based on an optimized protocol. An additional method, namely MSD V-Plex, was used to validate the proposed immunosensor, which is capable of multiplex detection of analytes, including cytokines, with higher sensitivity and a wider dynamic range compared with the conventional ELISA based on electrochemiluminescence technology.

The MSD V-Plex tests were performed in a laboratory accredited for clinical trials using serum samples obtained from the same 28 patients. The electrochemical results obtained from the clinical samples were validated with reference values confirmed using the commercial MSD V-Plex method based on the standard protocol used in the hospital (Table 1). The relative error between the two methods was less than 7.2%. Fig. 5g shows the correlation between the combined T3b/T4 PCa stage of IL-6 concentrations measured using the proposed immunosensor and the MSD V-Plex method. A linear regression model was built to determine the relationship between the two assays, which resulted in a line $y = 1.036\ x - 0.1430$, with a correlation coefficient of 0.997 (X, fiber-based developed immunosensor; Y, MSD V-Plex method). Figs. S9a and (b) show the correlation plots for stages T3b and T4 of PCa based on the real sample results between the proposed strategy and commercial method.

Additionally, we constructed a Bland–Altman plot to compare the statistical agreement between the two quantitative methods. As shown in Fig. 5h, all the values are within the 95% agreement interval and the mean bias is extremely close to zero, indicating no difference between the two methods, i.e., good consistency and clinical compatibility between them. Moreover, to confirm the statistical significance of IL-6 levels detected via the proposed immunosensor and the MSD V-Plex method, a paired *t*-test analysis was performed to evaluate the p-value.

Table 1
Comparison of IL-6 detection in clinical serum samples between proposed electrochemical sensor and commercial MSD V-Plex method.

S. No	PCa stages	MSD V-Plex method		Au/CF immunosensor	
		Mean value (pg/mL)	CV (%)	Mean value (pg/mL)	CV (%)
P1	T3b	4.42	2.50	4.53	3.24
P2	T3b	0.86	6.40	0.75	7.44
P3	T3b	0.72	3.90	0.84	4.34
P4	T3b	2.55	1.47	2.38	2.80
P5	T3b	1.09	3.30	1.10	1.03
P6	T3b	1.40	4.16	1.53	4.30
P7	T3b	7.31	1.21	7.57	1.50
P8	T3b	1.72	7.75	1.79	5.10
P9	T3b	1.26	4.52	1.40	4.9
P10	T3b	7.67	1.58	7.57	1.10
P11	T3b	3.79	2.80	3.66	2.94
P12	T3b	0.37	21.1	1.16	5.05
P13	T3b	0.72	6.72	0.78	6.40
P14	T3b	3.36	2.20	3.56	2.28
P15	T3b	0.79	4.67	0.81	6.70
P16	T3b	0.94	7.40	1.02	4.07
P17	T3b	0.61	12.5	0.89	6.08
P18	T3b	0.84	2.40	0.83	4.80
P19	T3b	1.55	2.70	1.66	1.71
P20	T3b	1.17	5.20	1.21	4.79
P21	T3b	1.96	2.22	2.02	3.25
P22	T3b	10.06	1.80	9.605	2.59
P23	T3b	1.93	4.00	1.924	3.20
P24	T4	0.85	4.60	0.88	2.49
P24	T4	2.23	2.80	2.12	2.66
P26	T4	1.70	3.50	1.82	3.14
P27	T4	2.64	3.30	2.72	2.61
P28	T4	7.25	1.50	6.98	2.41

Results of a two-tailed *t*-test show no statistically significant differences ($p > 0.5$) at the 95% confidence level between the two methods ($n = 28$) and an excellent correlation between them (Fig. 5h). These results indicate that the proposed Au/CFs modified immunosensor demonstrates high possibility for the detection of IL-6 in clinical samples. Considering these promising experimental results and information from the literature, it can be inferred that the developed fiber-based electrochemical immunosensor is promising for practical use and can be applied for IL-6 detection in real samples from patients with PCa.

4. Conclusion

In this study, we developed a low-cost electrochemical immunosensor to quantitatively detect IL-6 in clinical samples for the early diagnosis of PCa. A simple electrodeposition method was adopted to integrate electrochemically active Au nanostructures onto CFs for the immobilization of antibody probes to achieve highly sensitive and selective detections of IL-6. The excellent conductivity of the Au/CF nanocomposites assisted electron transfer and afforded large active sites for IL-6 antibody immobilization. Under optimized conditions, the developed fiber-based Au/CF immunosensor was demonstrated under a wide dynamic range (1 fg/mL to 1 μg/mL). It indicated a detection limit of 0.05 fg/mL and a sensitivity of 62.17 μA/(fg mL^{-1}), as well as exhibited superior selectivity when compared with the reactivity of coexistent species in the human serum. Additionally, the developed immunosensor demonstrated clinical significance and has been effectively applied for the detection and quantification of IL-6 in serum obtained from patients with PCa (stages T3b and T4). The results were validated using the commercial MSD V-Plex method in an accredited laboratory. The simplicity, easy preparation, and high efficiency of the developed strategy offer high reliability for the early prediction of PCa and other diseases and can thus be applied for detecting cancer biomarkers from clinical and POC devices.

CRediT authorship contribution statement

Sekar Madhu: Conceptualization, Methodology, Data curation, Investigation, Writing – original draft, Visualization, Writing – review & editing. **Jang Hee Han:** Formal analysis, Validation. **Chang Wook Jeong:** Formal analysis, Investigation, Validation. **Jungil Choi:** Conceptualization, Supervision, Investigation, Writing – review & editing, Funding acquisition, Project administration.

Declaration of competing interest

The authors declare that they have no known competing financial interests or personal relationships that could have appeared to influence the work reported in this paper.

Data availability

Data will be made available on request.

Acknowledgments

This study was supported by the Brain Pool program funded by the Ministry of Science and ICT through the National Research Foundation of Korea (NRF-2020H1D3A1A04077592), the National R&D Program for Cancer Control (HA17C0039), the new faculty research fund of Ajou University and a grant from the Patient-Centered Clinical Research Coordinating Center (HI19C0481 and HC19C0164). The biospecimens and data used in this study were provided by the Biobank of the Seoul National University Hospital, which is a member of the Korea Biobank Network (KBN4_A03). We thank Ja Hyeon Ku and Cheol Kwak at the Department of Urology at Seoul National University Hospital for providing patient samples.

Appendix A. Supplementary data

Supplementary data to this article can be found online at https://doi.org/10.1016/j.aca.2022.340644.

References

[1] E.B. Aydin, M. Aydin, M.K. Sezgintürk, The development of an ultra-sensitive electrochemical immunosensor using a PPyr-NHS functionalized disposable ITO sheet for the detection of interleukin 6 in real human serums, New J. Chem. 44 (2020) 14228–14238.
[2] Z. Culig, M. Puhr, Interleukin-6: a multifunctional targetable cytokine in human prostate cancer, Mol. Cell. Endocrinol. 360 (2012) 52–58.
[3] B. Wei, K. Mao, N. Liu, M. Zhang, Z. Yang, Graphene nanocomposites modified electrochemical aptamer sensor for rapid and highly sensitive detection of prostate specific antigen, Biosens. Bioelectron. 121 (2018) 41–46.
[4] B.A. Mahal, A.A. Aizer, J.A. Efstathiou, P.L. Nguyen, Association of very low prostate-specific antigen levels with increased cancer-specific death in men with high-grade prostate cancer, Cancer 122 (2016) 78–83.
[5] V. Michalaki, K. Syrigos, P. Charles, J. Waxman, Serum levels of IL-6 and TNF-α correlate with clinicopathological features and patient survival in patients with prostate cancer, Br. J. Cancer 90 (2004) 2312–2316.
[6] X. Guan, Cancer metastases: challenges and opportunities, Acta Pharm. Sin. B. 5 (2015) 402–418.
[7] W.J. Huss, R.J. Barrios, B.A. Foster, N.M. Greenberg, Differential expression of specific FGF ligand and receptor isoforms during angiogenesis associated with prostate cancer progression, Prostate 54 (2003) 8–16.
[8] G. Kabay, Y. Yin, C.K. Singh, N. Ahmad, S. Gunasekaran, M. Mutlu, Disposable electrochemical immunosensor for prostate cancer detection, Sensor. Actuator. B Chem. 360 (2022), 131667.
[9] L.H. Pan, S.H. Kuo, T.Y. Lin, C.W. Lin, P.Y. Fang, H.W. Yang, An electrochemical biosensor to simultaneously detect VEGF and PSA for early prostate cancer diagnosis based on graphene oxide/ssDNA/PLLA nanoparticles, Biosens. Bioelectron. 89 (2017) 598–605.
[10] E.B. Aydın, Highly sensitive impedimetric immunosensor for determination of interleukin 6 as a cancer biomarker by using conjugated polymer containing epoxy side groups modified disposable ITO electrode, Talanta 215 (2020), 120909.
[11] C. Russell, A.C. Ward, V. Vezza, P. Hoskisson, D. Alcorn, D.P. Steenson, D. K. Corrigan, Development of a needle shaped microelectrode for electrochemical detection of the sepsis biomarker interleukin-6 (IL-6) in real time, Biosens. Bioelectron. 126 (2019) 806–814.
[12] G.C. Fan, X.L. Ren, C. Zhu, J.R. Zhang, J.J. Zhu, A new signal amplification strategy of photoelectrochemical immunoassay for highly sensitive interleukin-6 detection based on TiO2/CdS/CdSe dual co-sensitized structure, Biosens. Bioelectron. 59 (2014) 45–53.
[13] G.J. Wise, V.K. Marella, G. Talluri, D. Shirazian, Cytokine variations in patients with hormone treated prostate cancer, J. Urol. 164 (2000) 722–725.
[14] R. Laocharoensuk, Development of electrochemical immunosensors towards point-of-care cancer diagnostics: clinically relevant studies, Electroanalysis 28 (2016) 1716–1729.
[15] C.K. Tang, A. Vaze, M. Shen, J.F. Rusling, High-throughput electrochemical microfluidic immunoarray for multiplexed detection of cancer biomarker proteins, ACS Sens. 1 (2016) 1036–1043.
[16] L.S.S. Kumar, X. Wang, J. Hagen, R. Naik, I. Papautsky, J. Heikenfeld, Label free nano-aptasensor for interleukin-6 in protein-dilute bio fluids such as sweat, Anal. Methods 8 (2016) 3440–3444.
[17] J. Homola, Present and future of surface plasmon resonance biosensors, Anal. Bioanal. Chem. 377 (2003) 528–539.
[18] T.H. Chou, C.Y. Chuang, C.M. Wu, Quantification of Interleukin-6 in cell culture medium using surface plasmon resonance biosensors, Cytokine 51 (2010) 107–111.
[19] G.A. Messina, N.V. Panini, N.A. Martinez, J. Raba, Microfluidic immunosensor design for the quantification of interleukin-6 in human serum samples, Anal. Biochem. 380 (2008) 262–267.
[20] K. Zhang, G. Liu, E.M. Goldys, Robust immunosensing system based on biotin-streptavidin coupling for spatially localized femtogram mL−1 level detection of interleukin-6, Biosens. Bioelectron. 102 (2018) 80–86.
[21] S. Singh, A.A.S. Gill, M. Nlooto, R. Karpoormath, Prostate cancer biomarkers detection using nanoparticles based electrochemical biosensors, Biosens. Bioelectron. 137 (2019) 213–221.
[22] L. Yang, H. Zhao, S. Fan, S. Deng, Q. Lv, J. Lin, C.P. Li, Label-free electrochemical immunosensor based on gold-silicon carbide nanocomposites for sensitive detection of human chorionic gonadotrophin, Biosens. Bioelectron. 57 (2014) 199–206.
[23] S. Chandra Barman, M. Sharifuzzaman, M.A. Zahed, C. Park, S.H. Yoon, S. Zhang, H. Kim, H. Yoon, J.Y. Park, A highly selective and stable cationic polyelectrolyte encapsulated black phosphorene based impedimetric immunosensor for Interleukin-6 biomarker detection, Biosens. Bioelectron. 186 (2021), 113287.
[24] S. Madhu, P. Manickam, M. Pierre, S. Bhansali, P. Nagamony, V. Chinnuswamy, Nanostructured SnO_2 integrated conductive fabrics as binder-free electrode for neurotransmitter detection, Sensors Actuators, A Phys. 269 (2018) 401–411.
[25] S. Madhu, A.J. Anthuuvan, S. Ramasamy, P. Manickam, S. Bhansali, P. Nagamony, V. Chinnuswamy, ZnO nanorod integrated flexible carbon fibers for sweat cortisol detection, ACS Appl. Electron. Mater. 2 (2020) 499–509.
[26] M. Sekar, M. Pandiaraj, S. Bhansali, N. Ponpandian, C. Viswanathan, Carbon fiber based electrochemical sensor for sweat cortisol measurement, Sci. Rep. 9 (2019) 1–14.
[27] I. Jeerapan, S. Poorahong, Review—flexible and stretchable electrochemical sensing systems: materials, energy sources, and integrations, J. Electrochem. Soc. 167 (2020), 037573.
[28] Y. Ko, M. Kwon, W.K. Bae, B. Lee, S.W. Lee, J. Cho, Flexible supercapacitor electrodes based on real metal-like cellulose papers, Nat. Commun. 8 (2017) 1–10.
[29] Z. Khorablou, F. Shahdost-Fard, H. Razmi, Flexible and highly sensitive methadone sensor based on gold nanoparticles/polythiophene modified carbon cloth platform, Sensor. Actuator. B Chem. 344 (2021), 130284.
[30] Z. Wang, S. Yang, Y. Wang, W. Feng, B. Li, J. Jiao, B. Han, Q. Chen, A novel oriented immunosensor based on AuNPs-thionine-CMWCNTs and staphylococcal protein A for interleukin-6 analysis in complicated biological samples, Anal. Chim. Acta 1140 (2020) 145–152.
[31] Q. Peng, Y. Zhang, S. Yang, T. Yuwen, Y. Liu, J. Fan, G. Zang, Glucose determination behaviour of gold microspheres-electrodeposited carbon cloth flexible electrodes in neutral media, Anal. Chim. Acta 1159 (2021), 338442.
[32] J. Song, L. Wang, H. Qi, H. Qi, C. Zhang, Highly selective electrochemical method for the detection of serotonin at carbon fiber microelectrode modified with gold nanoflowers and overoxidized polypyrrole, Chin. Chem. Lett. 30 (2019) 1643–1646.
[33] B. Zhang, M. Chen, J. Cao, Y. Liang, T. Tu, J. Hu, T. Li, Y. Cai, S. Li, B. Liu, J. Xu, B. Liang, X. Ye, X. Cai, An integrated electrochemical POCT platform for ultrasensitive circRNA detection towards hepatocellular carcinoma diagnosis, Biosens. Bioelectron. 192 (2021), 113500.
[34] Z. Yao, R. Yue, F. Jiang, C. Zhai, F. Ren, Y. Du, Electrochemical-reduced graphene oxide-modified carbon fiber as Pt-Au nanoparticle support and its high efficient electrocatalytic activity for formic acid oxidation, J. Solid State Electrochem. 17 (2013) 2511–2519.
[35] C. Oh, B. Park, C. Li, C. Maldarelli, J.L. Schaefer, T. Datta-Chaudhuri, P.W. Bohn, Electrochemical immunosensing of interleukin-6 in human cerebrospinal fluid and human serum as an early biomarker for traumatic Brain injury, ACS Meas. Sci. Au. 1 (2021) 65–73.
[36] S. Madhu, S. Ramasamy, P. Manickam, P. Nagamony, V. Chinnuswamy, TiO_2 anchored carbon fibers as non-invasive electrochemical sensor platform for the cortisol detection, Mater. Lett. 308 (2022), 131238.
[37] G. Qin, H. Zhang, H. Liao, Z. Li, J. Tian, Y. Lin, D. Zhang, Q. Wu, Novel graphene nanosheet-wrapped polyaniline rectangular-like nanotubes for flexible all-solid-state supercapacitors, J. Mater. Sci. 52 (2017) 10981–10992.
[38] A.T.E. Vilian, V. Veeramani, S.M. Chen, R. Madhu, C.H. Kwak, Y.S. Huh, Y.K. Han, Immobilization of myoglobin on Au nanoparticle-decorated carbon nanotube/

polytyramine composite as a mediator-free H_2O_2 and nitrite biosensor, Sci. Rep. 5 (2015) 1–10.
[39] T. Ngoc, T. Pham, Y.S. Yoon, Development of Nanosized Mn_3O_4-Co_3O_4 on Multiwalled Carbon Nanotubes for Cathode Catalyst in Urea Fuel Cell, vol. 13, 2020, p. 2322.
[40] M.R. Hasan, M.S. Ahommed, M. Daizy, M.S. Bacchu, M.R. Ali, M.R. Al-Mamun, M. A. Saad Aly, M.Z.H. Khan, S.I. Hossain, Recent development in electrochemical biosensors for cancer biomarkers detection, Biosens. Bioelectron. X. 8 (2021), 100075.
[41] H. Yamazaki, G. Suzuki, K. Masui, N. Aibe, D. Shimizu, T. Kimoto, K. Yoshida, S. Nakamura, H. Okabe, Radiotherapy for clinically localized T3b or T4 very-high-risk prostate cancer-role of dose escalation using high-dose-rate brachytherapy boost or high dose intensity modulated radiotherapy, Cancers 13 (2021) 1–13.